Auroral Processes Associated With Saturn's Moon Enceladus

D. A. Gurnett

Department of Physics and Astronomy, University of Iowa, Iowa City, Iowa, USA

W. R. Pryor

Science Department, Central Arizona College, Coolidge, Arizona, USA

Observations from the Cassini spacecraft have shown that Saturn's small moon Enceladus emits a geyser-like plume of water vapor and small icy particles from volcano-like vents in its southern polar region. It has also been shown that the interaction of this plume with the rapidly rotating magnetosphere of Saturn produces UV auroral emissions in Saturn's atmosphere near the foot of the moon's magnetic flux tube. Just how the charged particles responsible for the aurora are accelerated is a topic of considerable current interest. In this chapter, we give an overview of auroral processes associated with Enceladus. We show that the interaction of the plume with Saturn's corotating magnetospheric plasma leads to a wide variety of effects, including strong local distortions of the planetary magnetic field, the acceleration of electron beams, the generation of whistler mode radio emissions, and the excitation of a standing Alfvén wave that links Enceladus to Saturn's upper atmosphere. Many of these effects are similar to those observed near Jupiter's moon Io, which is known to produce auroral emissions near the foot of its magnetic flux tube, and to those occurring in the Earth's aurora.

1. INTRODUCTION

In early 2005, the Cassini spacecraft, which was placed in orbit around Saturn on 1 July 2004, began a series of close flybys of Saturn's moon Enceladus. This small icy moon has a radius of only 252 km and orbits Saturn near the equatorial plane at a radial distance of 3.95 R_S (radius of Saturn = 60,268 km). From previous images taken by Voyagers 1 and 2 during the 1980–1981 flybys of Saturn, it was known that the moon displayed evidence of geologic activity [*Smith et al.*, 1981]. Also, the maximum density of the *E* ring occurred near the orbit of Enceladus, which suggested that the moon is the source of the small micron-sized particles in this ring [*Stone and Owen*, 1984]. Despite this evidence that something unusual was occurring at Enceladus, it came as a surprise when strong magnetic field perturbations were observed near the moon during the first Cassini close flyby of Enceladus on 17 February 2005. The initial interpretation was that the magnetic field perturbations were due to the interaction of Saturn's rapidly corotating magnetosphere with a dense cloud of gas originating from the moon [*Dougherty et al.*, 2006]. This interpretation was subsequently confirmed by Cassini imaging observations that showed a geyser-like plume of material originating from a system of volcano-like vents near the south pole of the moon [*Porco et al.*, 2006]. Two images showing the sunlight scattered from small particles in the plume are shown in Figure 1. Several distinct plumes can be seen near the moon in the first image (Figure 1a), all originating from vents in the southern polar region. Figure 1b, which has enhanced sensitivity, shows that

Auroral Phenomenology and Magnetospheric Processes: Earth and Other Planets
Geophysical Monograph Series 197
© 2012. American Geophysical Union. All Rights Reserved.
10.1029/2011GM001174

Copyright © 2012. American Geophysical Union. All rights reserved.

Keiling, A., Donovan, E., Bagenal, F., & Karlsson, T. (Eds.). (2012). Auroral phenomenology and magnetospheric processes : Earth and other planets. Retrieved from http://ebookcentral.proquest.com
Created from uiowa on 2020-06-09 12:23:45.

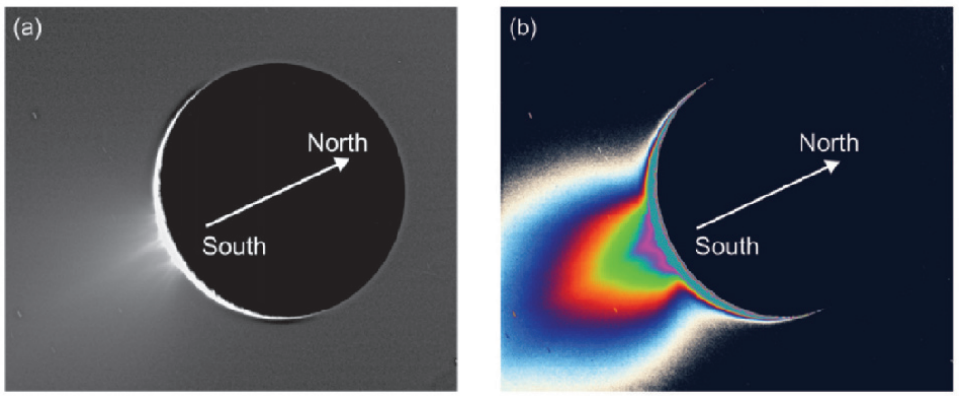

Figure 1. (a) High-phase angle clear-filter images taken by the Cassini Imaging Science Subsystem showing the plume of material ejected from the southern polar region of Enceladus. From *Porco et al.* [2006] (http://www.sciencemag.org/content/311/5766/1393.abstracta). Reprinted with permission from AAAS. (b) An enhanced color-coded version of Figure 1a.

the plume extends southward over a region that has vertical and horizontal extents comparable to the size of the moon.

Because of the remarkable processes occurring in and near Enceladus, the orbit of Cassini was subsequently adjusted to give a series of passes near and through the plume. UV absorption features observed in starlight that passed through the plume and in situ measurements of the small dust particles revealed that the plume is composed primarily of water vapor and micron and submicron water ice particles [*Hansen et al.*, 2006; *Spahn et al.*, 2006]. Mass spectrometer measurements showed that, in addition to water vapor, the plume also contains a wide range of heavier molecules, including complex hydrocarbons [*Waite et al.*, 2011]. Particle and field measurements showed that the plume has a very strong effect on the corotating magnetospheric plasma, which streams by at a nominal approach speed of 26.4 km s^{-1}. These effects include (1) charge exchange reactions between the neutral gas in the plume and the corotating magnetospheric ions, with the attendant acceleration of the newly created pickup ions to energies of several hundred eV by the corotational electric field [*Tokar et al.*, 2006], (2) local depletion of radiation belt particles due to impacts with the moon [*Jones et al.*, 2006], and (3) strong evidence that charged dust particles play an important role in the interaction [*Spahn et al.*, 2006; *Farrell et al.*, 2010; *Simon et al.*, 2011; *Kriegel et al.*, 2011; *Shafiq et al.*, 2011].

During the Voyager 1 flyby of Jupiter in 1979, it was discovered that its moon Io has active volcanism and that the resulting gas cloud around the moon interacts strongly with Jupiter's rapidly rotating magnetospheric plasma. Magnetic field measurements made during the Voyager 1 flyby of Io [*Ness et al.*, 1979; *Neubauer*, 1980] showed that a standing Alfvén wave (also called an Alfvén wing) is excited by the moon, thereby confirming a prediction made many years earlier by *Goldreich and Lynden-Bell* [1969] to explain Io's control of Jupiter's decametric radio emissions [*Bigg*, 1964]. Several years later, aurora emissions were observed in Jupiter's atmosphere near the foot of the Io flux tube [*Connerney et al.*, 1993; *Clarke et al.*, 1996], further demonstrating the strength of the Io interaction. The recent discovery of geysers at Enceladus prompted an intense search for similar effects at Saturn. Although an initial search for auroral emissions in Saturn's atmosphere near the foot of Enceladus' magnetic field line was unsuccessful [*Wannawichian et al.*, 2008], a more extensive search by *Pryor et al.* [2011] reported clear evidence of such emissions. Pryor et al. also identified magnetic field-aligned electron beams in the downstream wake of the moon with sufficient energy flux to drive the auroral emissions. At about the same time, *Gurnett et al.* [2011] reported observations of a standing Alfvén wave excited by Enceladus and of field-aligned electron beams and radio emissions originating from the vicinity of the moon. In this chapter, we give an overview of these and other auroral processes associated with Enceladus and compare these to similar processes at Io and in the Earth's auroral regions.

2. THE AURORA FOOTPRINT OF ENCELADUS

To search for aurora near the foot of Enceladus' magnetic flux tube, *Pryor et al.* [2011] used measurements from the Cassini Ultraviolet Imaging Spectrometer (UVIS). This instrument provides spectra in both the extreme ultraviolet (EUV) and the far ultraviolet (FUV) parts of the spectrum. The EUV and FUV channels have narrow 2 × 60 and 1.5 × 60 mrad fields of view. Spatial scans of Saturn's atmosphere were obtained by slewing the spacecraft. To provide the best

Copyright © 2012. American Geophysical Union. All rights reserved.

Keiling, A., Donovan, E., Bagenal, F., & Karlsson, T. (Eds.). (2012). Auroral phenomenology and magnetospheric processes : Earth and other planets. Retrieved from http://ebookcentral.proquest.com
Created from uiowa on 2020-06-09 12:23:45.

opportunity for detecting auroral emissions, the search was confined to times when Cassini was near periapsis at high latitudes over the mostly dark northern polar region. Of approximately 316 UV images of the region near the foot of Enceladus' flux tube, only 6 images were found with auroral spots of the right size and location to be associated with Enceladus. Two such images, obtained at subspacecraft latitudes from 74° to 65° and radial distances from 8.1 to 6.0 R_S, are shown in Figure 2. Figure 2a was taken from 02:16 to 03:28 UT on 26 August 2008, and Figure 2b was taken about an hour and a quarter later, from 03:38 to 04:50 UT. The bright circular emission at about 75° latitude is Saturn's auroral oval [*Gérard et al.*, 2004; *Grodent et al.*, 2011]. The bright spots marked by the white boxes at about 64.5°N latitude are emissions associated with Enceladus' flux tube. The boxes, which have widths of 4° in latitude and 10° in longitude, are centered on the magnetic field line through the center of Enceladus using the offset spin-aligned magnetic dipole model of *Burton et al.* [2009]. In computing these boundaries, the altitude of the emission was assumed to be 1100 km, which is the altitude that UV emissions are expected to be generated by auroral electrons impacting Saturn's mostly molecular hydrogen atmosphere [*Gérard et al.*, 2009]. As can be seen, the agreement with the predicted location of the UV emission is very good. The approximately 0.9 h shift in the local time of the auroral spot from Figure 1a to Figure 1b is caused by the orbital motion of Enceladus, which has a period of 1.37 days. Although the UV emissions are weaker and occur much less frequently than those associated with Io, these observations provide compelling evidence that Enceladus is exciting auroral emissions near the foot of its magnetic flux tube.

3. PARTICLE AND FIELD MEASUREMENTS NEAR ENCELADUS

At the time of this writing (31 October 2011), a total of 16 flybys of Enceladus have been carried out by Cassini. The flybys are designated E0 through E15. The flyby geometries are quite varied but primarily consist of two types: (1) passes obtained on equatorial orbits that are targeted to pass either upstream or downstream of the moon or, in some cases, offset to the north or south so as to pass over the poles and (2) passes on high inclination orbits that are designed to pass directly through the plume on steeply inclined north/south trajectories. Since it is not possible to describe all of the observations, we have decided to discuss two passes, E4 and E8, which provide a good overview of the observed phenomena. The spacecraft trajectories for these flybys are shown in Figure 3 using a corotational-aligned coordinate

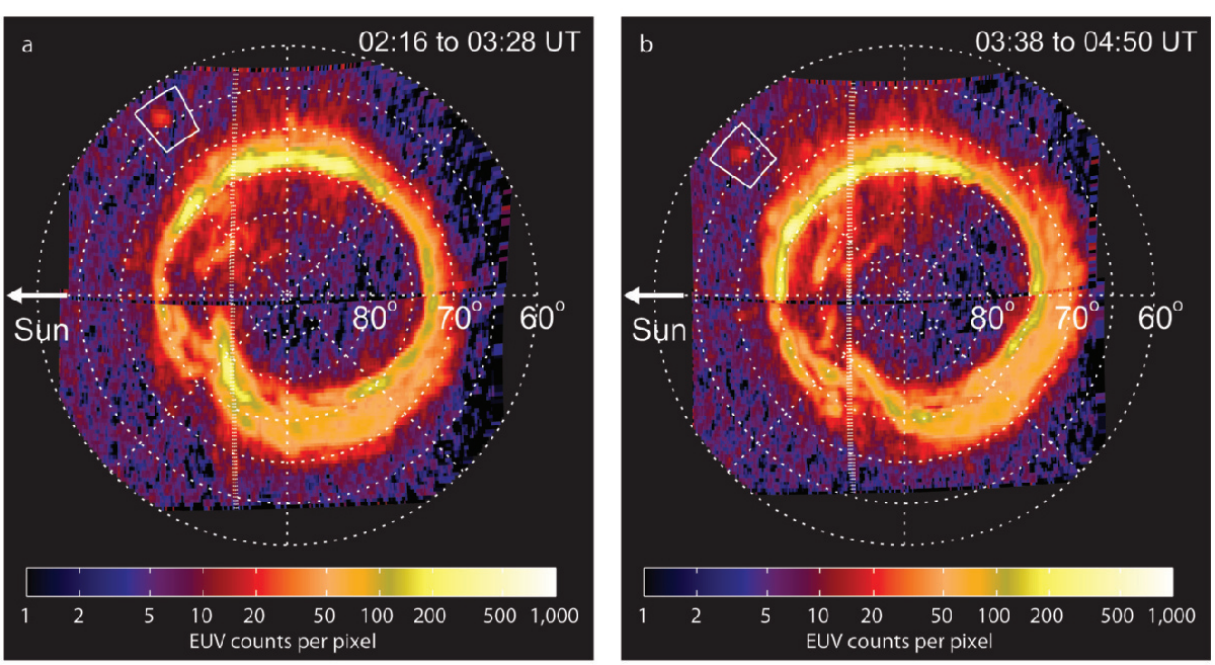

Figure 2. Two extreme UV images of the northern polar region obtained by the Ultraviolet Imaging Spectrometer on Cassini, separated by about an hour and a quarter on 26 August 2008. Reprinted by permission from Macmillan Publishers Ltd: *Nature* [*Pryor et al.*, 2011], copyright 2011.

Copyright © 2012. American Geophysical Union. All rights reserved.

Keiling, A., Donovan, E., Bagenal, F., & Karlsson, T. (Eds.). (2012). Auroral phenomenology and magnetospheric processes : Earth and other planets. Retrieved from http://ebookcentral.proquest.com
Created from uiowa on 2020-06-09 12:23:45.

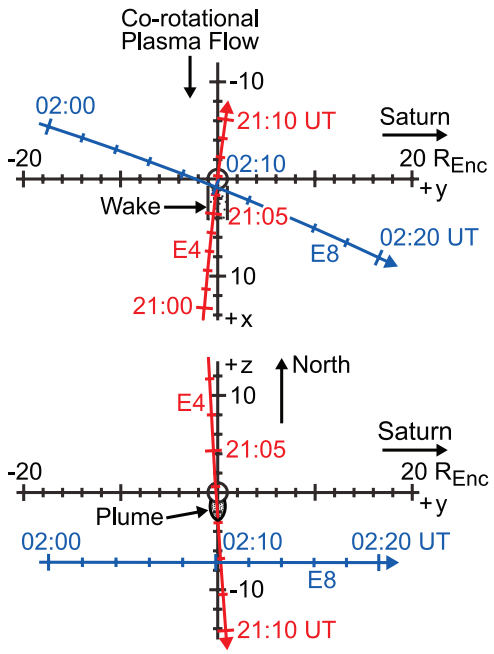

Figure 3. Spacecraft trajectories in an Enceladus-centered corotationally aligned coordinate system for the E4 and E8 flybys. The z axis is parallel to Saturn's rotational axis, the $+x$ axis is in the direction of the nominal corotational plasma flow, and the $+y$ axis, which is directed toward Saturn, completes the right-hand coordinate system.

system centered on the moon. One reason for selecting these two passes is that the field of view of the electron spectrometer (ELS), which is part of the Cassini plasma spectrometer (CAPS), was aligned nearly along the magnetic field direction. This orientation is desirable because field-aligned electron beams are expected to be the most likely source of the aurora at the foot of the magnetic field line. Very few flybys have this favorable orientation.

3.1. E4 Flyby

An overview of the particle and fields measurements obtained during the E4 flyby is shown in Figure 4. We start by discussing the electric field intensities detected by the radio and plasma wave science (RPWS) instrument. These are shown in Figure 4a, which gives a color-coded representation of the electric field intensities as a function of frequency and time. Although the RPWS instrument was designed to detect radio and plasma waves, the intense noise on the right side of the spectrogram is caused by dust particles striking the spacecraft. Because the spacecraft is moving at a very high velocity, ~17 km s^{-1}, relative to Enceladus (and to the dust particles), when a small particle strikes the spacecraft, it is instantly vaporized and ionized, thereby causing a rapidly expanding cloud of hot electrons that produces a voltage pulse on the RPWS electric antenna. A sample voltage pulse is shown by the small plot inserted in the spectrogram. The particle size threshold for detecting such impacts is believed to be a few microns. By counting the voltage pulses, the impact rate can be determined. Around the time of peak intensity (red in the spectrogram), roughly 21:06 to 21:08 UT, the impact rate is approximately 1300 impacts per second. As can be seen from the arrow marked "north-to-south equator crossing," the highest intensities occur in the region just south of the equator, consistent with passage through the plume as determined from optical observations. It is interesting to note that there is still a significant level of impulsive dust impact noise as early as 21:00 UT, more than 20 R_S north of the moon. Although most of the dust is concentrated in the plume, some dust is observed over a very large region around the moon.

Next, we describe the plasma and magnetic field measurements obtained during the E4 flyby. An energy-time spectrogram of the electron count rate detected by the CAPS ELS is shown in Figure 4b. The corresponding pitch angles detected by the ELS are shown in Figure 4c. These are generally less than about 20° to 30°, i.e., nearly field-aligned. As can be seen, very intense electron fluxes are present during the approach to the moon, from about 20:54 to 21:05 UT. From the spacecraft trajectory in Figure 3 and noting that the magnetic field is almost directly southward (see Figure 4d), one can see that the electron fluxes are occurring along magnetic field lines that pass through the downstream wake region. The electron energy spectrum has a bimodal distribution, with an intense narrow peak at about 1 keV, and a broader peak at about 10 eV. Both have substantial temporal variations. Since the spacecraft is north of the moon and the magnetic field is directed toward the south, the pitch angles are such that the electrons are moving upward toward the moon. The magnetic field measurements in Figure 4d show that large magnetic field disturbances are present in the region where the intense electron fluxes are observed, especially in the B_x component. A negative ΔB_x disturbance relative to the magnetic field model (shown by the dashed lines) is indicative of a magnetic field line that is draped around the moon due to mass loading, as discussed by *Dougherty et al.* [2006]. There are two regions with such a draped field configuration, the first indicated by the small negative ΔB_x disturbance from about 20:56:00 to 20:58:30 UT, nearly 20 R_E downstream of the moon, and the second indicated by the larger negative ΔB_x disturbance from about 21:04:30 to 21:07:00 UT, immediately downstream of the moon. In between these two disturbances, ΔB_x is positive, indicating an antidraped magnetic field. Just what causes these relatively large downstream magnetic field fluctuations

Copyright © 2012. American Geophysical Union. All rights reserved.

Keiling, A., Donovan, E., Bagenal, F., & Karlsson, T. (Eds.). (2012). Auroral phenomenology and magnetospheric processes : Earth and other planets. Retrieved from http://ebookcentral.proquest.com
Created from uiowa on 2020-06-09 12:23:45.

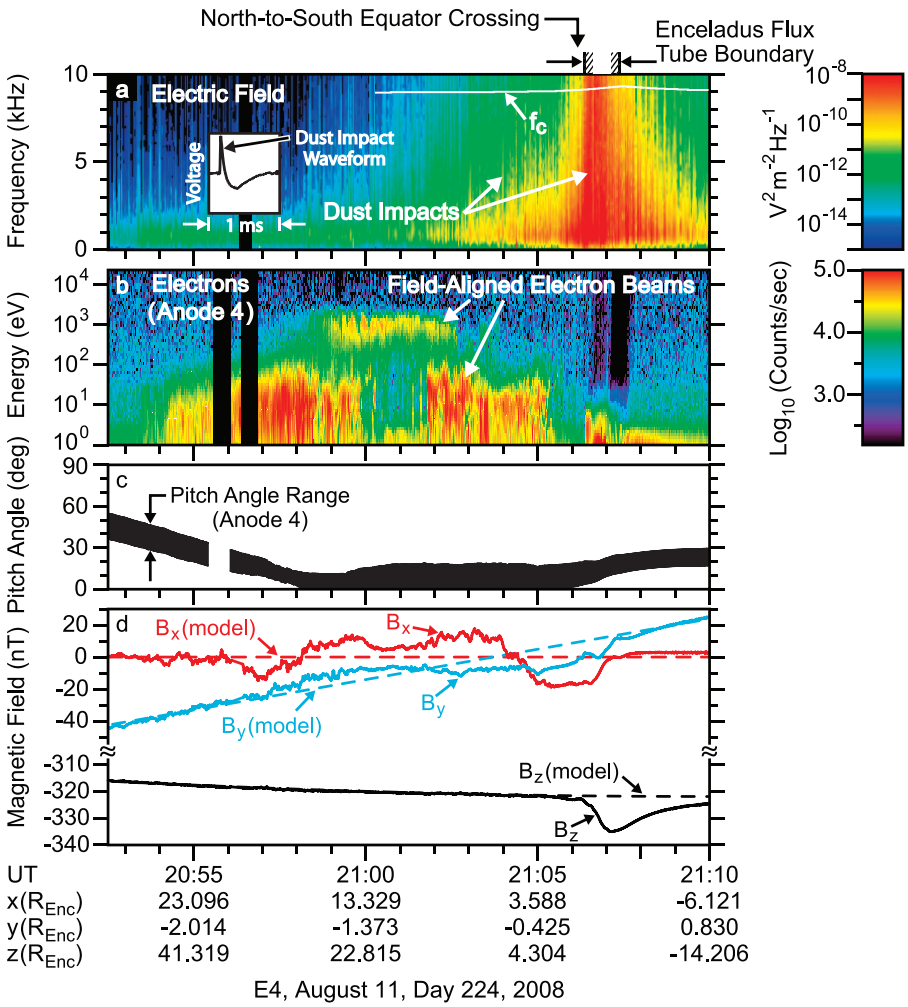

Figure 4. An overview of measurements obtained during the E4 flyby on 11 August 2008. (a) A frequency-time spectrogram of the electric field intensity detected by the radio and plasma wave science (RPWS) instrument. (b) An energy-time spectrogram of the electron count rate from the Cassini plasma spectrometer (CAP) electron spectrometer (ELS) and (c) The corresponding pitch angles. (d) A plot of the magnetic field components measured by the magnetometer (MAG).

is not known for certain. *Pryor et al.* [2011] suggested that they may be caused by Alfvén waves that are reflecting back and forth between the two hemispheres in the downstream region. However, they are also reminiscent of a downstream flow instability, such as the Kármán vortex street commonly seen downstream of a cylindrical object in a hydrodynamic flow.

3.2. E8 Flyby

An overview of the E8 particle and field measurements is shown in Figure 5, using the same basic format as in Figure 4. In sharp contrast to the E4 flyby, Figure 5a shows that there is relatively little evidence of dust impacts in the electric field spectrogram. This is because the E8 flyby is a relatively distant flyby, passing over the south pole of the moon at a radial distance of 7.2 R_S (see Figure 3). Although there are relatively few dust impacts, a very clearly defined V-shaped radio emission can be seen that has its apex centered almost exactly on the time of closest approach. This type of radio emission is commonly observed over the terrestrial auroral zones and is called "auroral hiss" because of its close association with the aurora [see *Gurnett*, 1966; *Gurnett et al.*, 1983]. The V-shaped frequency-time characteristic is a propagation effect that arises for whistler mode waves propagating at wave normal angles near the resonance

Copyright © 2012. American Geophysical Union. All rights reserved.

Keiling, A., Donovan, E., Bagenal, F., & Karlsson, T. (Eds.). (2012). Auroral phenomenology and magnetospheric processes : Earth and other planets. Retrieved from http://ebookcentral.proquest.com
Created from uiowa on 2020-06-09 12:23:45.

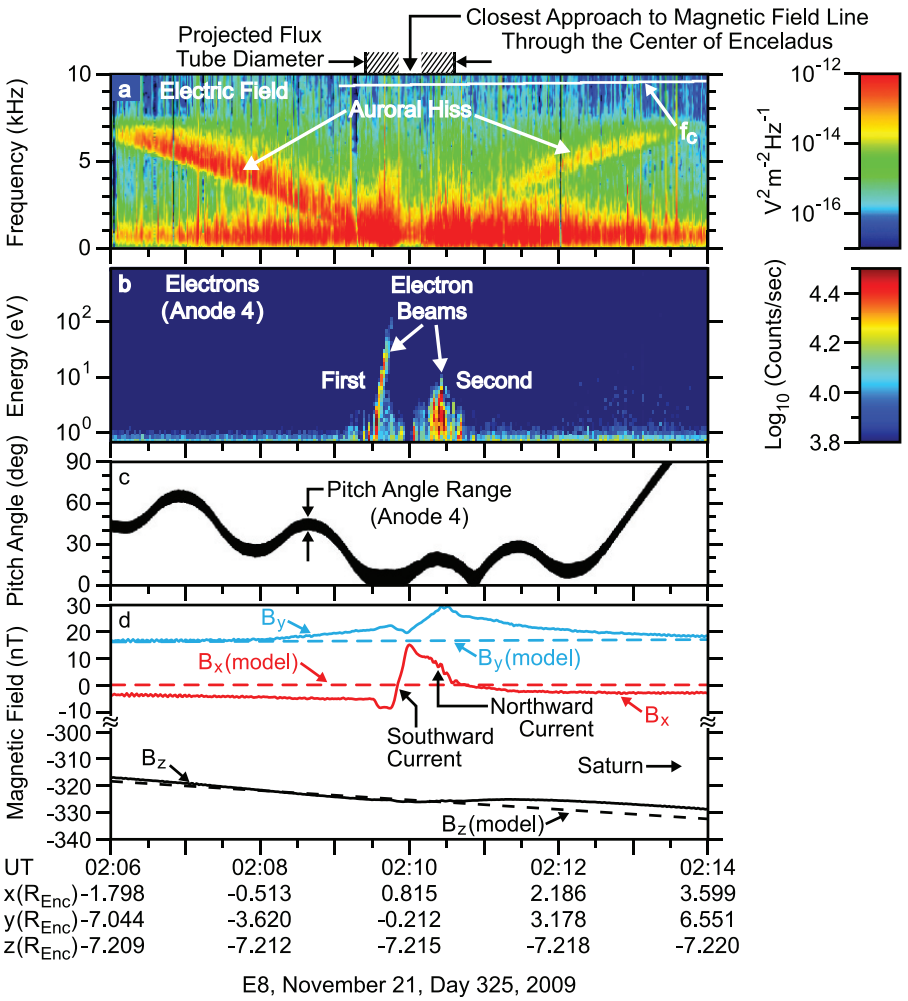

Figure 5. An overview of measurements obtained during the E8 flyby on 21 November 2009 using the format shown in Figure 4. (a) A frequency-time spectrogram of the electric field intensity detected by RPWS. (b) An energy-time spectrogram of the electron count rate from the CAP ELS and (c) the corresponding pitch angles. (d) A plot of the magnetic field components measured by the MAG. From *Gurnett et al.* [2011].

cone [*Mosier and Gurnett*, 1969; *James*, 1976]. It is well established that terrestrial auroral hiss is generated by field-aligned electron beams with energies ranging from a few tens of eV to several keV [*Ergun et al.*, 2003]. Indeed, the energy-time spectrogram in Figure 5b shows that two field-aligned electron beams are observed in the ELS data near the apex of the V-shaped emission. The magnetic field data in Figure 5d also show that two large oppositely directed ramp-like magnetic field disturbances occur in this same region. These ramp-like magnetic field variations are clearly indicative of field-aligned currents, first southward, from about 02:09:45 to 02:09:58 UT, followed almost immediately by a northward current, from 02:09:58 to 02:10:32 UT. This combination of two oppositely directed currents on a size scale comparable to the diameter of the moon provides strong evidence that the spacecraft passed directly through a shear-mode Alfvén wave excited by the moon. For a further discussion of the Alfvén wave interpretation, see *Gurnett et al.* [2011].

Studies of auroral hiss on Earth show that the emission is produced by an electron beam-plasma interaction [*Maggs*, 1976] at the Landau resonance velocity, $v_{\|} = \omega/k_{\|}$. Terrestrial studies also show that auroral hiss can be used as a remote sensing tool to determine where the electron beam is accelerated [*Mosier and Gurnett*, 1969; *James*, 1976; *Ergun et al.*, 2003]. This technique relies on the fact that for whistler mode propagation near the resonance cone, the wave energy propagates at a known angle to the magnetic field. For the

Copyright © 2012. American Geophysical Union. All rights reserved.

Keiling, A., Donovan, E., Bagenal, F., & Karlsson, T. (Eds.). (2012). Auroral phenomenology and magnetospheric processes : Earth and other planets. Retrieved from http://ebookcentral.proquest.com
Created from uiowa on 2020-06-09 12:23:45.

plasma parameters that exist near Enceladus, where the electron cyclotron frequency is much less than the electron plasma frequency, $f_c \ll f_p$, the angle of the ray path, ψ, relative to the magnetic field is given by the simple equation, $\sin \psi = f/f_c$, where f is the wave frequency. From this equation, one can see that the radiation from a point source is beamed along a cone-shaped surface, the opening angle of which increases with increasing frequency. It is this frequency dependence that gives the auroral hiss its characteristic V-shaped frequency-time dependence, first decreasing in frequency as the spacecraft approaches the magnetic field line through the source and then increasing as the spacecraft moves away. Since the magnetic field is known to a very good approximation in the region around the moon, it is a straightforward procedure to determine a source position that gives a good fit to the V-shaped frequency-time spectrum. Figure 6 shows the results of such a fitting procedure. Figure 6a shows the ray paths that give the best fits to the inbound and outbound branches of the V-shaped emission, and Figure 6b shows the quality of the fits, which are very good. The y' axis used in this analysis passes through the center of the moon and is parallel to the trajectory in the x,y plane [see *Gurnett et al.*, 2011]. As can be seen, both the inbound and outbound sources are located very close to the moon, slightly south and slightly downstream, consistent with a source in or very near the plume.

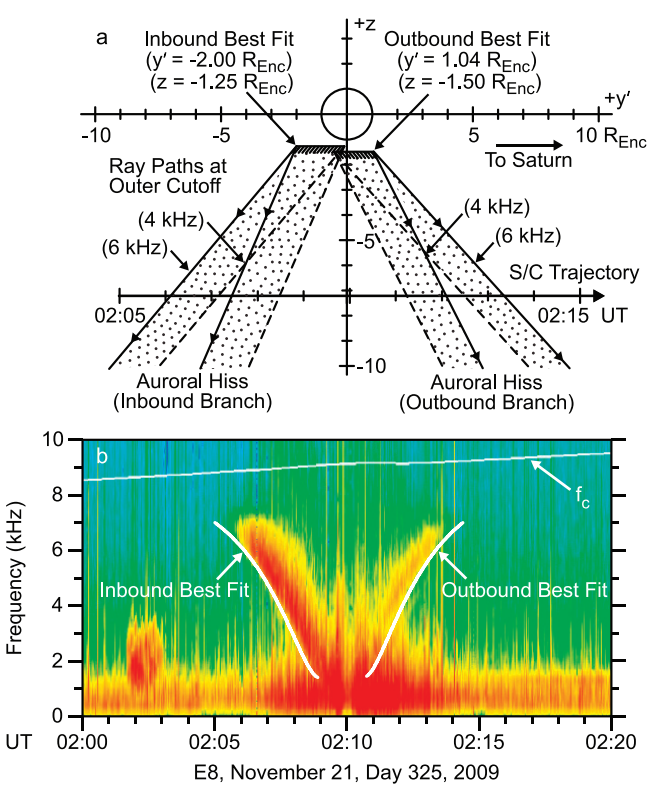

Figure 6. (a) Best-fit ray paths for the inbound and outbound branches of the V-shaped auroral hiss emission in Figure 5a and (b) corresponding best fits to the outer envelopes of the auroral hiss spectrum. From *Gurnett et al.* [2011].

4. DISCUSSION

We have described Cassini observations of aurora at the foot of the Enceladus flux tube and particle and field measurements from two close flybys of the moon that are relevant to the processes responsible for producing the aurora. The E4 flyby, which was on magnetic field lines that intersected the downstream wake, showed very intense field-aligned electron beams with energies ranging from about 10 eV to 1 keV. The beams, which are highly variable, extend over a considerable region downstream of the moon with peak energy fluxes of 1 to 2 mW m^{-2}. The field of view of the electron detector was such that it only detected electrons moving up the magnetic field line toward the moon, with no measurements in the opposite direction. Therefore, it is not clear whether the electrons are being accelerated toward the moon by some acceleration process farther down the field line near Saturn or whether they consist of magnetically reflected bidirectional beams accelerated near the moon, such as those observed by *Williams et al.* [1996] downstream of Io. In contrast, the E8 flyby, which was a distant pass over the south pole of the moon, clearly showed two field-aligned electron beams arriving from the moon. Whistler mode auroral hiss was also observed during this pass that is almost certainly generated by these beams. Ray path analyses of the auroral hiss showed that the source of these emissions, and by inference, the region where the electron beams are being accelerated, was located very close to the moon, probably in or near the plume. For a further discussion see the work of *Gurnett et al.* [2011]. Although models of the plasma interaction by *Saur et al.* [2007], *Wannawichian et al.* [2008], *Kriegel et al.* [2009], *Jia et al.* [2010], and others had suggested that an Alfvén wave might be excited by the interaction of the corotating plasma with the moon, the E8 flyby, for the first time, clearly showed that a standing Alfvén wave is, in fact, generated by Enceladus. Whether the electron beams are directly related to the Alfvén wave is not clear. The beam observed from 02:10:05 to 02:10:40 UT is in the correct location and direction to carry the northward current associated with the Alfvén wave. However, the relationship of the other beam, from 02:09:30 to 02:09:45 UT, to the Alfvén wave is not so clear, since it occurs in a region where there appears to be little or no current.

Although electron beams with significant energies and intensities have been observed in the vicinity of Enceladus,

Copyright © 2012. American Geophysical Union. All rights reserved.

Keiling, A., Donovan, E., Bagenal, F., & Karlsson, T. (Eds.). (2012). Auroral phenomenology and magnetospheric processes : Earth and other planets. Retrieved from http://ebookcentral.proquest.com
Created from uiowa on 2020-06-09 12:23:45.

it is not yet clear how they are accelerated or whether they are able to reach Saturn's atmosphere with enough energy to produce the observed aurora intensities. In fact, since the beams observed during the E4 and E8 flybys were in substantially different locations relative to the moon (downstream versus near the flux tube through the moon), it is not clear that the acceleration mechanisms are even related. For the intense beams observed moving upward on the downstream magnetic field lines during the E4 flyby, it is not known whether they can reach Saturn's atmosphere even if they have a bidirectional distribution. Although the beams were described as "field-aligned" by *Pryor et al.* [2011], the atmospheric loss cone has an angle of only 6°. Since the angular resolution of the measurements is only about 15° to 20° (see Figure 4c), one cannot be certain that a sufficient fraction of the observed energy flux, ~1 to 2 mW m^{-2}, can actually reach the foot of the field line to produce the observed aurora. For the beams observed in association with the standing Alfvén wave during the E8 flyby, there are similar uncertainties. The ray path studies of the auroral hiss observed during the E8 flyby strongly indicate that these beams are accelerated very close to Enceladus, probably in or near the plume. Since the beams observed during the E8 flyby are considerably less energetic than those observed during the E4 flyby, it is doubtful that they have enough energy to produce the aurora. We can only speculate how the electrons observed during the E8 flyby are accelerated. Possible acceleration mechanisms might include (1) electron inertial or kinetic effects associated with the Alfvén wave [*Lysak and Song*, 2003; *Watt and Rankin*, 2008], (2) parallel electric fields [*Knight*, 1973] that develop in the Alfvén wave current system, or (3) electrical effects produced by charged dust in the plume [*Kriegel et al.*, 2011; *Morooka et al.*, 2011]. In considering the origin of the aurora, one must also consider the electromagnetic energy flux carried by the Alfvén wave. For the observed amplitude of the magnetic field perturbation associated with the Alfvén wave, $\Delta B \sim 12$ nT, and the nominal plasma parameters observed during the E8 flyby ($B_0 = 325$ nT, $n = 47$ cm^{-3}, ion mass ~ 18 amu), the wave energy flux at the foot of the magnetic field line is estimated to be about 4 mW m^{-2}, which is quite significant, greater than the energy flux of the electron beams observed during the E4 flyby. This Alfvén wave energy could very well be converted to electron beam energy as the wave propagates downward and interacts with Saturn's ionosphere. For a discussion of possible processes for converting the Alfvén wave energy to field-aligned electron beams, see the work of *Hess et al.* [2011].

Acknowledgments. The research at the University of Iowa was supported by JPL contract 1415150 and the research at Central Arizona College was supported by the college, by a JPL Cassini subcontract to LASP/University of Colorado, and by a Cassini Data Analysis Program grant to Space Environment Technologies.

REFERENCES

Bigg, E. K. (1964), Influence of the satellite Io on Jupiter's decametric emission, *Nature*, *203*, 1008–1010, doi:10.1038/2031008a0.

Burton, M. E., M. K. Dougherty, and C. T. Russell (2009), Model of Saturn's internal planetary magnetic field based on Cassini observations, *Planet. Space Sci.*, *57*, 1706–1713, doi:10.1016/j.pss.2009.04.008.

Clarke, J. T., et al. (1996), Far-ultraviolet imaging of Jupiter's aurora and the Io footprint, *Science*, *274*, 404–409, doi:10.1126/science.274.5286.404.

Connerney, J. E. P., R. L. Baron, T. Satoh, and T. Owen (1993), Images of excited H_3^+ at the foot of the Io flux tube in Jupiter's atmosphere, *Science*, *262*, 1035–1038, doi:10.1126/science.262.5136.1035.

Dougherty, M. K., K. K. Khurana, F. M. Neubauer, C. T. Russell, J. Saur, J. S. Leisner, and M. E. Burton (2006), Identification of a dynamic atmosphere at Enceladus with the Cassini magnetometer, *Science*, *311*, 1406–1409, doi:10.1126/science.1120985.

Ergun, R. E., C. W. Carlson, J. P. McFadden, R. J. Strangeway, M. V. Goldman, and D. L. Newman (2003), Fast auroral snapshot satellite observations of very low frequency saucers, *Phys.Plasmas*, *10*, 454–462, doi:10.1063/1.1530160.

Farrell, W. M., W. S. Kurth, R. L. Tokar, J.-E. Wahlund, D. A. Gurnett, Z. Wang, R. J. MacDowall, M. W. Morooka, R. E. Johnson, and J. H. Waite Jr. (2010), Modification of the plasma in the near-vicinity of Enceladus by the enveloping dust, *Geophys. Res. Lett.*, *37*, L20202, doi:10.1029/2010GL044768.

Gérard, J.-C., D. Grodent, J. Gustin, A. Saglam, J. T. Clarke, and J. T. Trauger (2004), Characteristics of Saturn's FUV aurora observed with the Space Telescope Imaging Spectrograph, *J. Geophys. Res.*, *109*, A09207, doi:10.1029/2004JA010513.

Gérard, J.-C., B. Bonfond, J. Gustin, D. Grodent, J. T. Clarke, D. Bisikalo, and V. Shematovich (2009), Altitude of Saturn's aurora and its implications for the characteristic energy of precipitated electrons, *Geophys. Res. Lett.*, *36*, L02202, doi:10.1029/2008GL036554.

Goldreich, P., and D. Lynden-Bell (1969), Io, a Jovian unipolar inductor, *Astrophys. J.*, *156*, 59–78, doi:10.1086/149947.

Grodent, D., J. Gustin, J.-C. Gérard, A. Radioti, B. Bonfond, and W. R. Pryor (2011), Small-scale structures in Saturn's ultraviolet aurora, *J. Geophys. Res.*, *116*, A09225, doi:10.1029/2011JA016818.

Gurnett, D. A. (1966), A satellite study of VLF hiss, *J. Geophys. Res.*, *71*(23), 5599–5615, doi:10.1029/JZ071i023p05599.

Gurnett, D. A., S. D. Shawhan, and R. R. Shaw (1983), Auroral hiss, *Z* mode radiation, and auroral kilometric radiation in the polar magnetosphere: DE 1 observations, *J. Geophys. Res.*, *88*(A1), 329–340, doi:10.1029/JA088iA01p00329.

Copyright © 2012. American Geophysical Union. All rights reserved.

Keiling, A., Donovan, E., Bagenal, F., & Karlsson, T. (Eds.). (2012). Auroral phenomenology and magnetospheric processes : Earth and other planets. Retrieved from http://ebookcentral.proquest.com
Created from uiowa on 2020-06-09 12:23:45.

Gurnett, D. A., et al. (2011), Auroral hiss, electron beams and standing Alfvén wave currents near Saturn's moon Enceladus, *Geophys. Res. Lett.*, *38*, L06102, doi:10.1029/2011GL046854.

Hansen, C. J., L. Esposito, A. I. F. Stewart, J. Colwell, A. Hendrix, W. Pryor, D. Shemansky, and R. West (2006), Enceladus' water vapor plume, *Science*, *311*, 1422–1425, doi:10.1126/science.1121254.

Hess, S. L. G., P. A. Delamere, V. Dols, and L. C. Ray (2011), Comparative study of the power transferred from satellite-magnetosphere interactions to auroral emissions, *J. Geophys. Res.*, *116*, A01202, doi:10.1029/2010JA015807.

James, H. G. (1976), VLF saucers, *J. Geophys. Res.*, *81*(4), 501–514.

Jia, Y.-D., C. T. Russell, K. K. Khurana, G. Toth, J. S. Leisner, and T. I. Gombosi (2010), Interaction of Saturn's magnetosphere and its moons: 1. Interaction between corotating plasma and standard obstacles, *J. Geophys. Res.*, *115*, A04214, doi:10.1029/2009JA014630.

Jones, G. H., E. Roussos, N. Krupp, C. Paranicas, J. Woch, A. Lagg, D. G. Mitchell, S. M. Krimigis, and M. K. Dougherty (2006), Enceladus' varying imprint on the magnetosphere of Saturn, *Science*, *311*, 1412–1415, doi:10.1126/science.1121011.

Knight, S. (1973), Parallel electric fields, *Planet. Space Sci.*, *21*, 741–750, doi:10.1016/0032-0633(73)90093-7.

Kriegel, H., S. Simon, J. Müller, U. Motschmann, J. Saur, K.-H. Glassmeier, and M. K. Dougherty (2009), The plasma interaction of Enceladus: 3D hybrid simulations and comparison with Cassini MAG data, *Planet. Space Sci.*, *57*, 2113–2122, doi:10.1016/j.pss.2009.09.025.

Kriegel, H., S. Simon, U. Motschmann, J. Saur, F. M. Neubauer, A. M. Persoon, M. K. Dougherty, and D. A. Gurnett (2011), Influence of negatively charged plume grains on the structure of Enceladus' Alfvén wings: Hybrid simulations versus Cassini Magnetometer data, *J. Geophys. Res.*, *116*, A10223, doi:10.1029/2011JA016842.

Lysak, R. L., and Y. Song (2003), Kinetic theory of the Alfvén wave acceleration of auroral electrons, *J. Geophys. Res.*, *108*(A4), 8005, doi:10.1029/2002JA009406.

Maggs, J. E. (1976), Coherent generation of VLF hiss, *J. Geophys. Res.*, *81*(10), 1707–1724.

Morooka, M. W., J.-E. Wahlund, A. I. Eriksson, W. M. Farrell, D. A. Gurnett, W. S. Kurth, A. M. Persoon, M. Shafiq, M. André, and M. K. G. Holmberg (2011), Dusty plasma in the vicinity of Enceladus, *J. Geophys. Res.*, *116*, A12221, doi:10.1029/2011JA017038

Mosier, S. R., and D. A. Gurnett (1969), VLF measurements of the Poynting flux along the geomagnetic field with the Injun 5 satellite, *J. Geophys. Res.*, *74*(24), 5675–5687, doi:10.1029/JA074i024p05675.

Ness, N. F., M. H. Acuna, R. P. Lepping, L. F. Burlaga, K. W. Behannon, and F. M. Neubauer (1979), Magnetic field studies at Jupiter with Voyager 1: Preliminary results, *Science*, *204*, 982–987, doi:10.1126/science.206.4421.966.

Neubauer, F. M. (1980), Nonlinear standing Alfvén wave current system at Io: Theory, *J. Geophys. Res.*, *85*(A3), 1171–1178, doi:10.1029/JA085iA03p01171.

Porco, C. C., et al. (2006), Cassini observes the active south pole of Enceladus, *Science*, *311*, 1393–1401, doi:10.1126/science.1123013.

Pryor, W. R., et al. (2011), The Enceladus auroral footprint at Saturn, *Nature*, *472*, 331–333, doi:10.1038/nature09928.

Saur, J., F. M. Neubauer, and N. Schilling (2007), Hemisphere coupling in Enceladus' asymmetric plasma interaction, *J. Geophys. Res.*, *112*, A11209, doi:10.1029/2007JA012479.

Shafiq, M., J.-E. Wahlund, M. W. Morooka, W. S. Kurth, and W. M. Farrell (2011), Characteristics of the dust-plasma interaction near Enceladus' south pole, *Planet. Space Sci.*, *59*, 17–25, doi:10.1016/j.pss.2010.10.006.

Simon, S., J. Saur, H. Kriegel, F. M. Neubauer, U. Motschmann, and M. K. Dougherty (2011), Influence of negatively charged plume grains and hemisphere coupling currents on the structure of Enceladus' Alfvén wings: Analytical modeling of Cassini magnetometer observations, *J. Geophys. Res.*, *116*, A04221, doi:10.1029/2010JA016338.

Smith, B. A., et al. (1981), Encounter with Saturn: Voyager 1 imaging science results, *Science*, *212*, 163–191, doi:10.1126/science.212.4491.163.

Spahn, F., et al. (2006), Cassini dust measurements at Enceladus and implications for the origin of the *E*-ring, *Science*, *311*, 1416, doi:10.1126/science.1121375.

Stone, E. C., and T. C. Owen (1984), The Saturn system, in *Saturn*, edited by T. Gehrels and M. S. Matthews, p. 15, Univ. of Ariz. Press, Tucson.

Tokar, R. L., et al. (2006), The interaction of the atmosphere of Enceladus with Saturn's plasma, *Science*, *311*, 1409–1412, doi:10.1126/science.1121061.

Waite, J. H., et al. (2011), Enceladus' plume composition, paper presented at the EPSC/DPS Joint Meeting 2011, Eur. Planet. Network, Nantes, France, 2–7 Oct.

Wannawichian, S., J. T. Clarke, and D. H. Pontius Jr. (2008), Interaction evidence between Enceladus' atmosphere and Saturn's magnetosphere, *J. Geophys. Res.*, *113*, A07217, doi:10.1029/2007JA012899.

Watt, C. E. J., and R. Rankin (2008), Electron acceleration and parallel electric fields due to kinetic Alfvén waves in plasma with similar thermal and Alfvén speeds, *Adv. Space Res.*, *42*, 964–969, doi:10.1016/j.asr.2007.03.030.

Williams, D. J., B. H. Mauk, R. E. McEntire, E. C. Roelof, T. P. Armstrong, B. Wilken, J. G. Roederer, S. M. Krimigis, T. A. Fritz, and L. J. Lanzerotti (1996), Electron beams and ion composition measured at Io and in its torus, *Science*, *274*, 401–403, doi:10.1126/science.274.5286.401.

D. A. Gurnett, Department of Physics and Astronomy, University of Iowa, Iowa City, IA 52242, USA. (donald-gurnett@uiowa.edu)

W. R. Pryor, Science Department, Central Arizona College, Coolidge, AZ 85128, USA.

Copyright © 2012. American Geophysical Union. All rights reserved.

Keiling, A., Donovan, E., Bagenal, F., & Karlsson, T. (Eds.). (2012). Auroral phenomenology and magnetospheric processes : Earth and other planets. Retrieved from http://ebookcentral.proquest.com
Created from uiowa on 2020-06-09 12:23:45.

Copyright © 2012. American Geophysical Union. All rights reserved.

Keiling, A., Donovan, E., Bagenal, F., & Karlsson, T. (Eds.). (2012). Auroral phenomenology and magnetospheric processes : Earth and other planets. Retrieved from http://ebookcentral.proquest.com
Created from uiowa on 2020-06-09 12:23:45.

Copyright © 2012. American Geophysical Union. All rights reserved.

Keiling, A., Donovan, E., Bagenal, F., & Karlsson, T. (Eds.). (2012). Auroral phenomenology and magnetospheric processes : Earth and other planets. Retrieved from http://ebookcentral.proquest.com
Created from uiowa on 2020-06-09 12:23:45.

Copyright © 2012. American Geophysical Union. All rights reserved.

Keiling, A., Donovan, E., Bagenal, F., & Karlsson, T. (Eds.). (2012). Auroral phenomenology and magnetospheric processes : Earth and other planets. Retrieved from http://ebookcentral.proquest.com
Created from uiowa on 2020-06-09 12:23:45.